UNITED NATIONS UNIVERSITY
GEOTHERMAL TRAINING PROGRAMME
Orkustofnun, Grensasvegur 9,
IS-108 Reykjavik, Iceland

Reports 2010
Number 28

PREFEASIBILITY DESIGN OF A 2×25 MW SINGLE-FLASH GEOTHERMAL POWER PLANT IN ASAL, DJIBOUTI

Hamoud Souleiman Cheik
Ministry of Energy and Natural Resources
P.O. Box 10010,
Djibouti
REPUBLIC OF DJIBOUTI
hamoudsoulei@yahoo.fr

ABSTRACT

Geologically, the most active area in Djibouti is the Asal area. Six wells have been drilled with varying depths ranging from 1137 to 2105 m. The first two wells were drilled in 1975 and the other four between 1987 and 1988. Well Asal-2 was damaged. The temperature of the other wells ranges from 260 to 360°C. In spite of significant geothermal studies and deep drilling explorations conducted since 1970 on several geothermal prospect zones, geothermal energy in Djibouti has yet to be developed. However, the process of developing a new power plant, using the steam resources from the wells, is now underway. The main objectives of this paper are to make a prefeasibility design of a geothermal power plant with a total net output power of 2×25 MWe. The purpose of modelling and simulation is to observe the performance of the system when a number of parameters, such as wet-bulb temperature and cooling water supply system, are changed. Also, the model provides a tool with which to determine the optimum and adequate pressure for the technical operation of the system and to optimise the electrical power production process. The simulation and technical analysis, using the EES program, has proven very useful for calculations, giving a turbine power output of 55.6 MWe and the power plant's electrical consumption as approximately 7.2% of the power from the turbine.

1. INTRODUCTION

Located in East Africa with an area of approximately 23,000 km^2, Djibouti is bordered on the east by the Gulf of Aden, on the southeast by Somalia, on the south and west by Ethiopia and on the north by Eritrea. It is strategically located at the mouth of the Bab el Mandeb strait, which links the Red Sea with the Gulf of Aden.

Geologically, Djibouti lies at the junction of three active, major coastal spreading centres: the East Africa Rift System, the Red Sea Rift and the Gulf of Aden. The rift zone is still expanding by about one millimetre per year. This unique geographical area is characterised by the presence of geothermal resources revealed by numerous hot springs and fumaroles found in different parts of the country (Figure 1). Geothermal prospecting started in Djibouti in 1970; different geothermal studies were conducted on several geothermal prospect zones. The exploration areas are in different stages and this is summarised in Table 1.

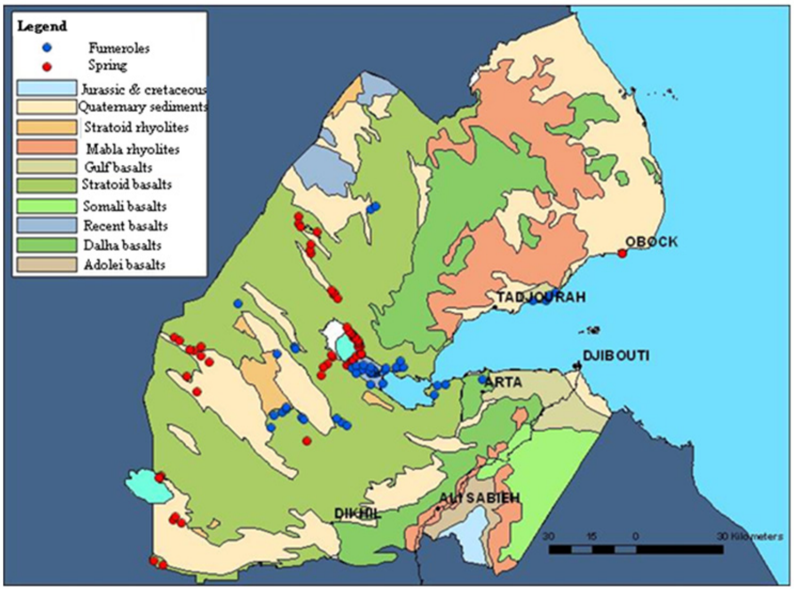

FIGURE 1: Djibouti, geology and geothermal surface manifestations (Jalludin, 2009)

TABLE 1: Geothermal prospects and exploration
(plusses (+) indicate stage of exploration, on a scale from 1 to 3)

	Exploration stage				Surface manifestations	
Area	**Geology**	**Geochemistry**	**Geophysics**	**Deep drilling**	**Hot springs**	**Fumaroles**
Asal	+++	++	+++	++	++	+
N-Ghoubbet	++	++	++		+	+
Gaggadé	++	++			+	+++
Hanlé	++	++	++	+		++
Lake Abbé	++	++			++	++
Arta	++	++	++			+
Obock		++			+	++
Alol	+	+			++	+

Geothermal exploration has shown the existence of a number of potential areas suited to electric power development. The total geothermal potential is estimated up to 900 MW (8 sites). The most important geothermal prospect in Djibouti, the Asal prospect (alternative spelling: Assal), is on an active rift zone that extends from the Ghoubbet al Kharab through Lake Asal.

The combined electricity generation potential of the three Asal geothermal systems (Gale le Goma, Fiale and South of Asal Lake) is estimated to be between 115 and 329 MWe (Elmi and Axelsson, 2010). In 2007, REI (Reykjavik Energy Invest) was granted an exploration license in the Asal Rift to build a 50 MWe initial plant and to later extend it to 100-150 MWe. The drilled wells in the Fiale area will be expected to contribute towards generation of the first 50 MWe.

In this report, the main purpose is a prefeasibility design of a 2x25 MWe single-flash geothermal power plant in Asal (Gale de Goma) in Djibouti. The report is made up of three parts:

- Knowledge of the field and wells (geology, geophysics, geochemistry, etc.) and the problems encountered;
- Thermodynamic analysis and method overview; and
- Discussion and conclusion.

2. THE ASAL GEOTHERMAL FIELD

Djibouti is almost entirely covered by volcanic rocks and thermal manifestations are widespread. The most active structure is the "Asal Rift".

2.1 Geology

The Asal Rift is the westward prolongation of the Gulf of Aden - Gulf of Tadjoura Ridge. It has a NW-SE trend and submerges in a southeast direction into the Ghoubbet Gulf and in a northeast direction into Lake Asal (160 m below sea level, the lowest point in Africa). It represents the landward prolongation of the oceanic spreading axis of the Gulf of Aden and is bounded by two systems of opposite-facing faults (Figure 2).

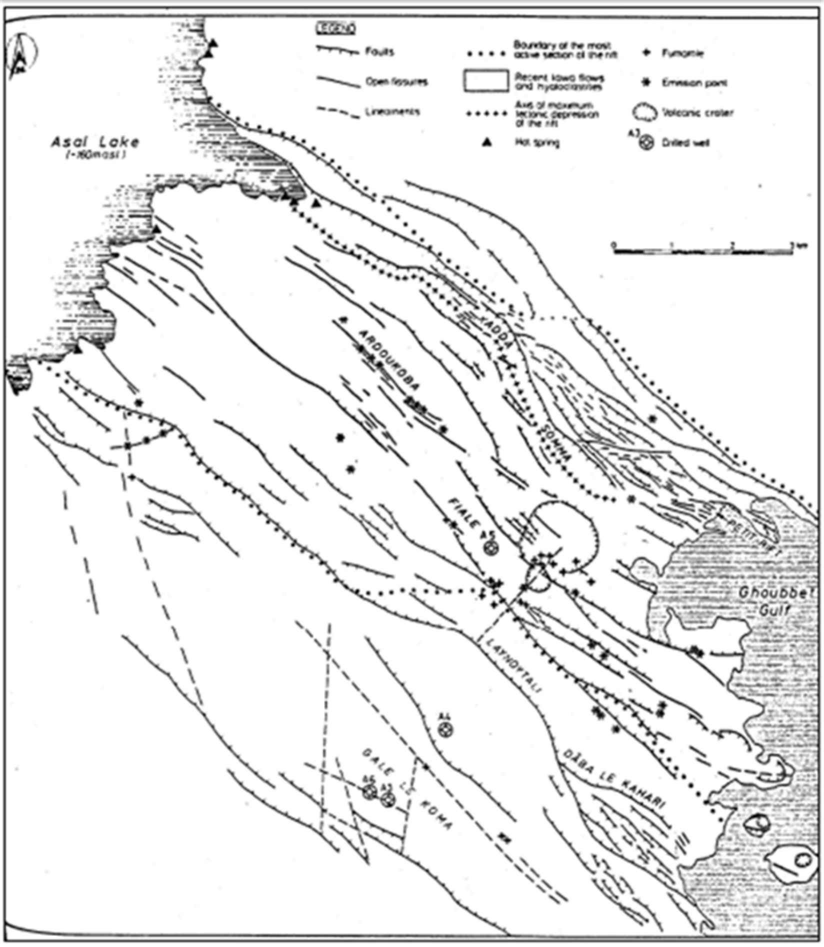

FIGURE 2: Structural map of the Asal area (Aquater, 1989)

The Asal area constitutes an oceanic rift (analogue to the black smokers), with a highly developed graben structure displaying axial volcanism. It is markedly asymmetrical with respect to its median line. The most intense magmatic activity is shifted northeast; even farther northeast these shifts are shown by the axis of the rift of maximum depression and by the zone with the most intense tectonic activity, close to the rift's northeast border. Thus, the rift's axis of crustal divergence seems to migrate from southwest to northeast; the migration of tectonic activity foreruns volcanic migration (Jalludin, 2009)

The most common volcanic formations in the Asal area are basalts locally interbedded by sedimentary levels of clays, lacustrine deposits and secondary conglomerates. The basaltic formations and contacts between various lava flows were originally permeable but the strong deposition of secondary minerals sealed the formation, thus making it impermeable.

The formations, crossed by the wells drilled, are related to the main volcanic units that outcrop in the area (Figure 3). These are, from top to bottom, as follows (Jalludin, 2009)

- Asal series, consisting of recent porphyritic basalts and hyaloclastites.
- Afar stratoid series (1-4 Ma) mainly consisting of basalts. In the upper part of the series, a thick layer of Pleistocene clays is underlain by an acidic, rhyolitic level.
- Pliocene clays.
- Dalha basalts series (4-8 Ma), consisting of basaltic products, with sedimentary intercalations.

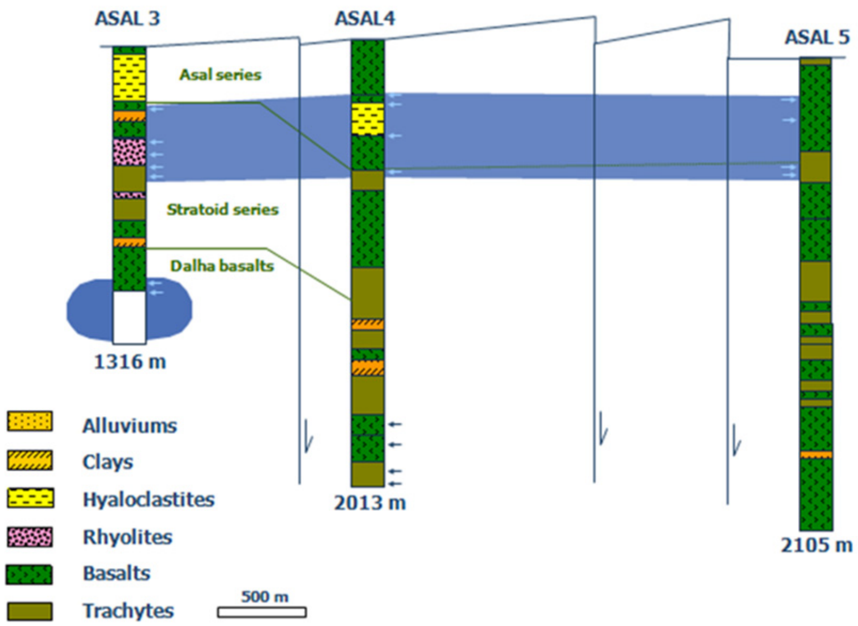

FIGURE 3: Stratigraphy of cross-section of the Asal field (Jalludin, 2009); the thickness of the recent Asal series increases towards the centre of the rift and the old Dalha series probably

2.2 Geophysics

All studies conducted between 1970 and today led to the recognition of three independent geothermal systems in the Asal region. The map in Figure 4 shows the location of these systems (Gale le Goma, Fiale and South of Lake). Figure 4 also shows the resistivity at 3000 m b.s.l., inferred lineaments in low-resistivity (red lines), seismicity (dark green dots) and geothermal surface manifestations (light green) (Árnason et al., 1988). The two super saline and sealed-off Gale Le Goma and South of Asal Lake systems are indicated, as is the more open, lower salinity Fiale system under Lava Lake.

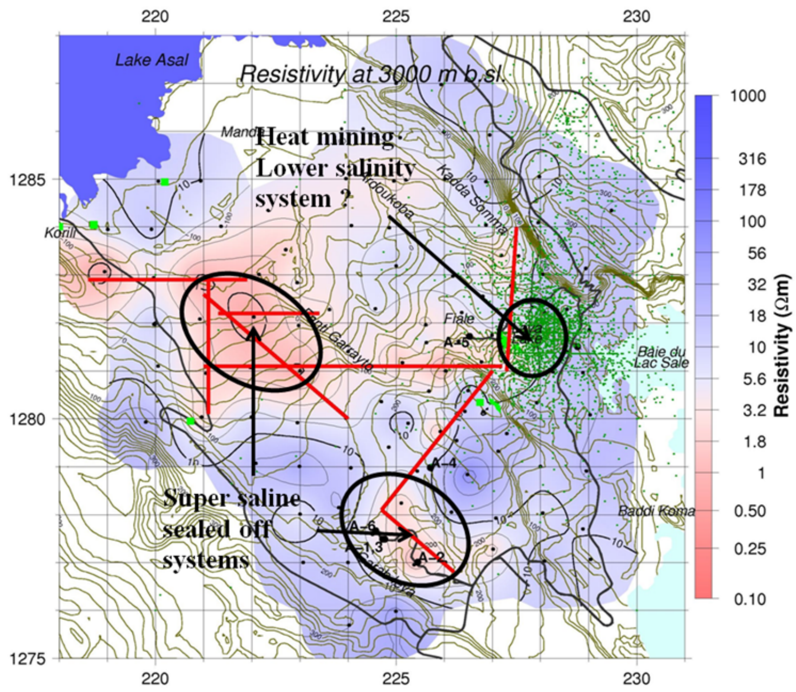

FIGURE 4: Resistivity at 3000 m b.s.l. (Elmi and Axelsson, 2010)

2.3 Geochemistry

The salinity of the deep reservoir fluid in the Asal geothermal field is high (120 g/l), about 3.5 times more saline than seawater. Fluids discharged from wells Asal 3 and Asal 6 indicate a rather acidic condition (pH 4-6) (Aquater, 1989). The results of a chemical analysis of fluids from well Asal 3 are reported in Table 2 (Ármannsson and Hardardóttir, 2010).

The chemistry of the fluids from the three wells that were tested, A1, A3 and A6, is very similar indicating that they draw from the same aquifer. The fluid is extremely saline, suggesting evaporated seawater. The major constituent composition of three deep water samples collected during the 1989-1990 flow test showed total dissolved solids (TDS) in the range of 115,000-121,000 mg/kg, Cl 67,000-71,000 mg/kg, Na 25,000-28,000 mg/kg and Ca 15,000-16,000 mg/kg. It was observed that, depending on the temperature at which seawater interacts with surrounding rocks, as well as on the water-rock contact period, there was a difference in the ionic content of the fluids compared to seawater.

TABLE 2: Properties and chemical composition of total fluid in well A-3 (modified from Ármannsson and Hardardóttir, 2010)

Property / Constituent	Measurement	Comparison to sea water (35‰)
Temperature, T	260°C	
Enthalpy, H	1,133 kJ/kg	
Pressure, P_0	20.4 bar	
pH	4.1	
SiO_2	460 ppm	6.4
Na	26,471 ppm	10,800
K	4,451 ppm	392
Ca	15,031 ppm	411
Mg	21.5 ppm	1,290
SO_4	12.4 ppm	2,712
Cl	70,979 ppm	19,800
F	4.85 ppm	1.3
Al	1.50 ppm	0.001
Fe	32.3 ppm	0.003
Zn	37 ppm	0.005
Pb	2.6 ppm	
Sr	161 ppm	8.1
B	9.09 ppm	4.5
Mn	116 ppm	0.0004
Cu	0.27 ppm	0.0009
Ni	<0.1 ppm	
CO_2	3,205 ppm	
H_2S	0.84 ppm	
NH_3	5.65 ppm	
H_2	0.57 ppm	
CH_4	1.51 ppm	
N_2	451 ppm	
TDS	116,344 ppm	

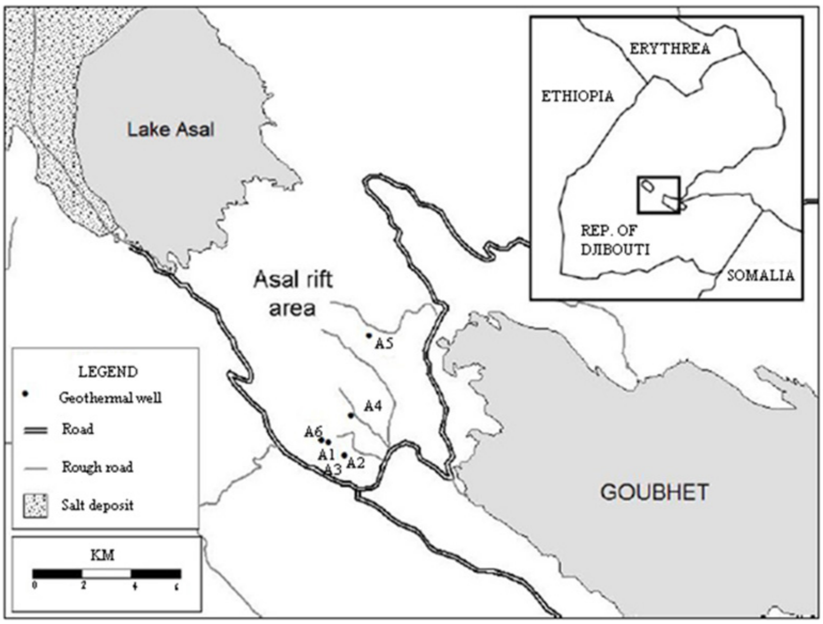

FIGURE 5: Well locations in the Asal geothermal field (Elmi and Axelsson, 2010)

According to a preliminary study of A3, and the analysis of scaling deposits in A6, as reported by Aquater (1989) in its final report, the fluid discharge from these wells resulted in such a large amount of solid deposits as to seriously compromise well production (see Sections 2.4.1 and 2.4.2).

2.4 Well productivity data

A total of six wells have been drilled in this area between 1975 and 1988. The three boreholes, Asal 1, 3 and 6, are located in the southern zone of the Asal rift inside the half circle of hyaloclastites known as Gale le Koma (Elmi, 2005). About 40 m separate wells Asal 1 and Asal 3. The distance between Asal 3 and 6 is approximately 300 m along a line striking NW-SE. Wells Asal 4 and 5 are located toward the central part of the rift (Figure 5). Asal 5 was drilled in the Inner Rift, about 1 km west of Lava Lake. Asal 4 is located about 2 km north-northeast of the site of Asal 3 and 6, close to a NW-SE fracture. Well Asal 2 is located 800 m southeast of the Asal 3 site (Aquater, 1989).

Wells A3 and A6 encountered the same reservoir as A1 with temperatures of 260-280°C. Well A4 showed temperatures close to the boiling curve below 200 m b.s.l., with a temperature close to 350°C at the bottom. Well A5 showed sharply increasing temperature below 200 m b.s.l., with a maximum of about 180°C at 500 m depth (Figure 6). Below that, the rocks are drastically cooled down compared to alteration mineralogy, with temperatures as low as 60-70°C at 900-1000 m depth. After that, the temperature rises steeply with depth and reaches about 360°C at the bottom. Wells A4 and A5 showed very little permeability and could not be flow-tested (Aquater, 1989).

Three wells were discharge tested: A1, A3 and A6 (Aquater, 1989, Virkir-Orkint, 1990). Measurements showed total well flow in the range of 20-60 kg/s. The best producer is A3 which, under stabilized conditions, has produced about 40 kg/s of fluid, 4-5 kg/s of which is steam. A three month test of the well showed a significant decline in production that was interpreted as being due to the formation of deposits in the pipes, thus hampering the flow (Figure 6). The enthalpy of the fluid was in the range 1069-1090 kJ/kg. A pressure connection was found between wells A3, A2 and A6, but wells A4 and A5 did not respond to the flow testing of A3. The reservoir permeability thickness product (kh) was found to be in the range of 7-11 Dm and an average porosity of 5% or less was indicated. The size of the drainage area for well A3 was observed to be in the range 7-9 km2 (Virkir-Orkint, 1990).

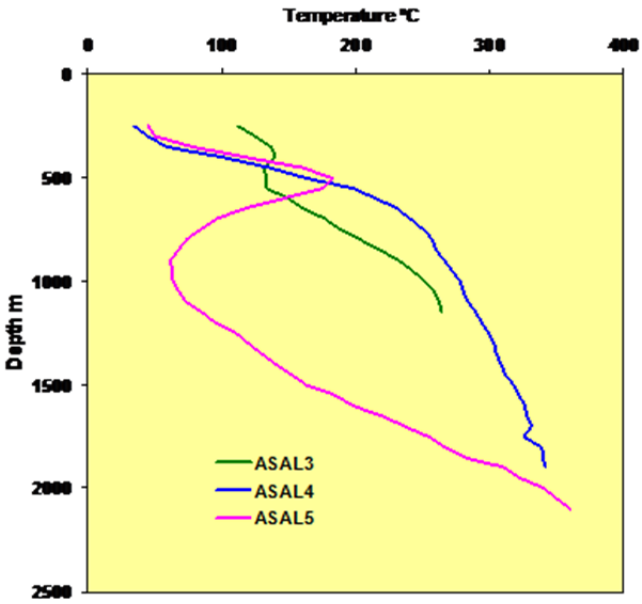

FIGURE 6: Temperature profiles of wells A3, A4 and A5 (Jalludin, 2009)

The geothermal exploration programs of the Asal area, including field studies and exploration drilling between 1970 and 1990, revealed high salinity, a deep Asal geothermal reservoir, the temperature profile and other potential geothermal areas (Table 3).

TABLE 3: Characteristics of Asal wells

Drilled Wells	Beginning of drilling	End of drilling	Final depth (m)	Temperature maximum (°C)	Total mass (ton/h)	Salinity (g/l)
Asal 1	9-03-1975	6-06-1975	1146	260	130 (WHP= 6 bar)	120
Asal 2	4-07-1975	15-09-1975	1554	235	-	-
Asal 3	11-06-1987	11-08-1987	1316	260	350 (WHP= 12.5 bar)	130
Asal 4	15-09-1987	20-12-1987	2013	345	-	-
Asal 5	7-01-1988	7-03-1988	2105	359	-	-
Asal 6	8-04-1988	10-06-1988	1761	280	150	130

2.4.1 Scale deposition

From October 1989 to April 1990, Virkir-Orkint carried out a comprehensive scaling/corrosion study in Asal (Virkir-Orkint, 1990). Certain patterns could be discerned by the distance from the wellhead, deposition at different pressures and possibly the environment of the deposition. In Table 4, the analysis of 7 samples from different sampling locations in A3 is reported. The analytical results were normalised to a sum of 100%.

Thus, it can be seen that the composition differs greatly according to the distance from the wellhead; sulphides, mostly galena, become more prominent close to the wellhead but silicates, and finally silica, become more prominent further away from the wellhead. In A3, scales of significant concentrations of carbonate (0.5-2.2% as CO_2), characterised as siderite, were also found. The distance from the wellhead does not tell the whole story. A sample from an orifice at the opening of the separator line in A3 contained galena almost exclusively. The thickness of the scale is also pressure dependent and an experiment on the separator line in A3 showed a significant increase in the scaling rate, between 17.7 and 16.2 bar (Figure 7), the increase being concomitant with a large increase in iron silicate deposition. Iron silicates start precipitating at temperatures below about 200°C (15.5 bar_a) but, at lower temperatures (<150°C), amorphous silica precipitation becomes prominent (Ármannsson and Hardardóttir, 2010).

TABLE 4: Chemical composition of scales from well A3 (Virkir-Orkint, 1990)

Constituent	WH	OR[1]	TP	SP[1]	BP[1]	SS	WB
P_0 (bar)	20.0	17.7	17.7	17.7	17.7	0	0
SiO_2 (%)	19.6	0	6.7	40.7	30.5	56.4	72.9
Al_2O_3 (%)	3.7	0	1.0	4.3	3.4	8.6	2.7
Fe_2O_3 (%)	22.5	0	6.7	31.8	25.8	14.8	2.7
MnO (%)	2.3	0	0.9	5.8	3.7	0.7	0.2
MgO (%)	1.6	0	0.1	0.7	1.1	0.2	0.2
CaO (%)	0.6	0	0.6	1.6	1.4	8.4	12.8
Na_2O (%)	4.4	0	0.3	1.4	1.7	8.1	0.8
K_2O (%)	0.1	0	0	0.7	0.4	1.9	2.9
S (%)	13.7	14.9	18.3	4.0	8.0	0.2	0.4
Cu (%)	0.4	0	0	0.1	0	0.1	0.1
Pb (%)	22.3	85.1	65.4	7.2	23.3	0.2	0.4
Zn (%)	8.8	0	0	1.7	1.0	0.4	0.1

[1] Some inhomogeneities (> ±10%). WH: Wellhead; OR: 90 mm orifice to separator line; TP: Two-phase pipe on separator line; SP: Separator; BP: Brine pipe; SS: Single drum silencer; WB: Weir box

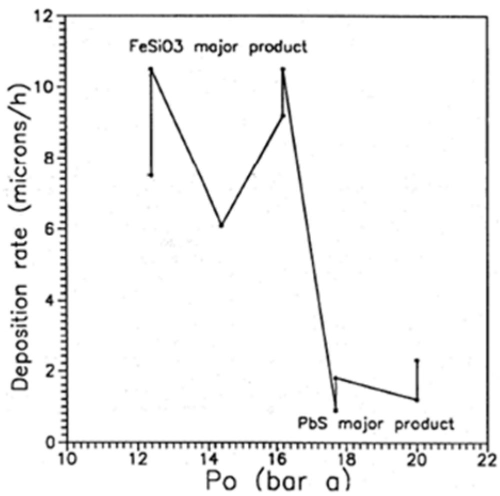

FIGURE 7: Thickness of scales on coupons at different pressures (Ármannsson and Hardardóttir, 2010)

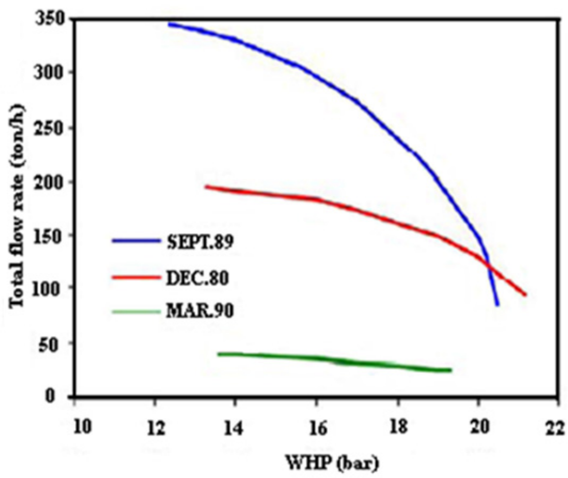

FIGURE 8: Output characteristic curves for different tests, well Asal 3 (Jalludin, 2009)

Scaling and reservoir pressure drop explain the decrease in the flowrate (Figure 8 and 9). At the flash zone between 650 and 750 m, the diameter of the wellbore was reduced by about 20 mm. And between 600 m and the wellhead, the diameter reduction was around 15 mm. At low pressure in surface equipment, the main deposition was $FeSiO_3$ and at high pressure (i.e. down in the well) it was galena PbS (Elmi, 2005).

After long term production tests, it was observed that the third and second deliverability curves decreased in comparison to the first one. Deposition of galena scale inside well Asal 3, while working at a high pressure between 18 and 20 bar_a, reduced the well radius and so decreased the discharge rate.

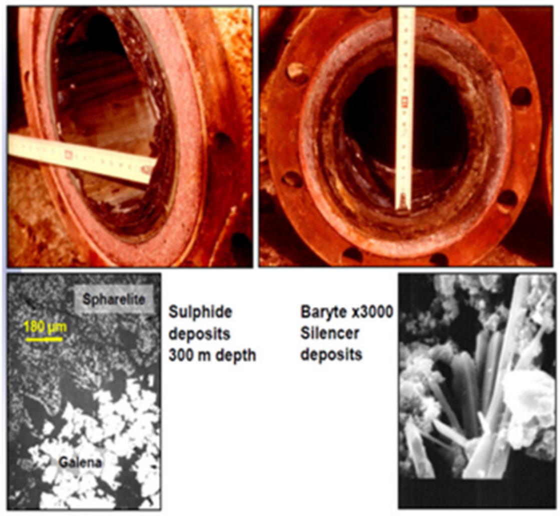

FIGURE 9: Scale deposits in 6” production liner, Asal 1 geothermal well (Jalludin, 2009)

2.4.2 Scale prevention and recommendations

As has been observed, the extent of iron silicate scaling in Asal is small above 16 bars; the recommendation is to keep the wellhead pressure well above that. Amorphous silica scales similarly are best avoided by keeping the separator pressure of the power plant above that of amorphous silica saturation. The sulphide and iron silicate scales may be dealt with by inhibition, but the amorphous silica deposits must be handled by pressure (temperature) control (Ármannsson and Hardardóttir, 2010).

3. THEORETICAL ANALYSIS AND METHOD OVERVIEW

In order to extract as much energy as possible from the geothermal fluid, a single-flash cycle has been proposed for this study (Figure 10). Schematic models of the power plant, with or without the use of a cooling tower, and EES equations for calculations of the models are presented in Appendix I.

3.1 Flash steam system process

The starting point for a thermodynamic analysis of a steam power cycle is the geothermal well. Wellhead pressure, mass flow and the saturation temperature of water characterise a geothermal well. From the saturation temperature of the water at the bottom of the well, one can calculate the enthalpy at the top as a function of wellhead pressure. The flashing process is assumed isenthalpic as no work or heat interactions take place during the process. This is denoted by the following equation:

$$h_1 = h_2 \tag{1}$$

3.2 Separator process

The function of the steam separator is to separate the geothermal fluid into two phases, vapour and liquid (Figure 11). The process of an ideal separator is to obtain at the outlets the saturated water and

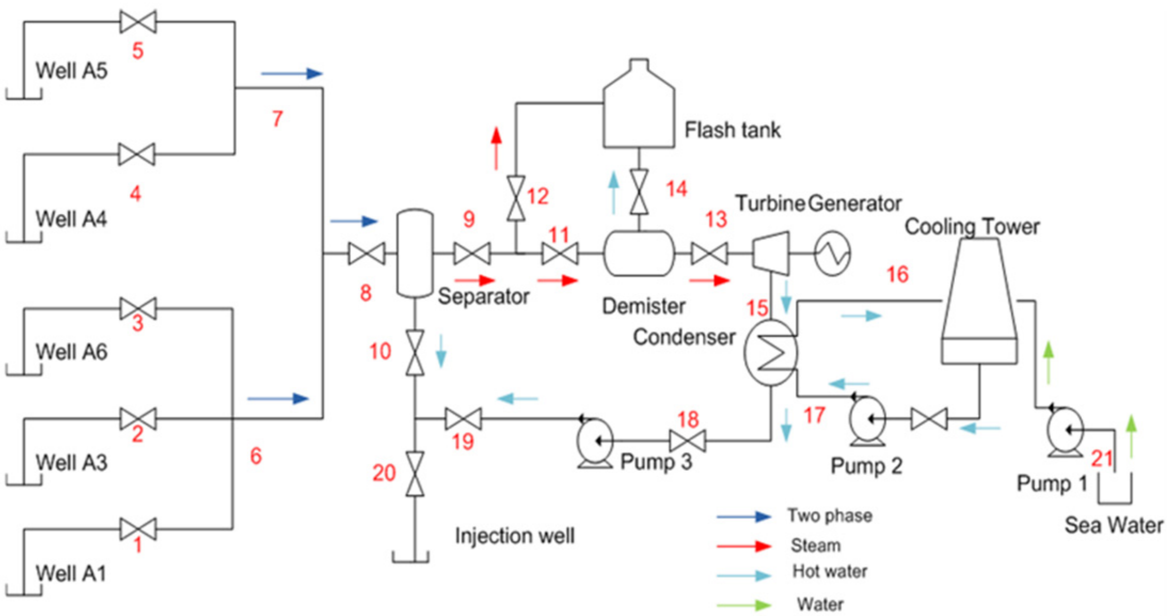

FIGURE 10: Flow diagram of Asal geothermal power plant

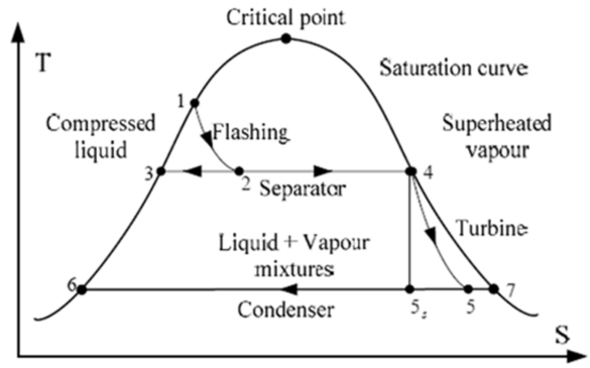

FIGURE 11: Temperature-entropy state diagram for single flash plant (Bandoro, 2006)

the saturated steam. The separation process is assumed to be isobaric. The pressures at points 8, 9 and 10 in Figure 10 are equivalent and the same as the separator pressure. The mass flow at point 8 equals the sum of the mass flow of points 9 and 10 according to mass balance (Figure 12). The steam fraction (in the two-phase flow) to the separator is given by

$$x_8 = \frac{h_8 - h_{10}}{h_9 - h_{10}} \tag{2}$$

where indices refer to number labels in Figure 10.

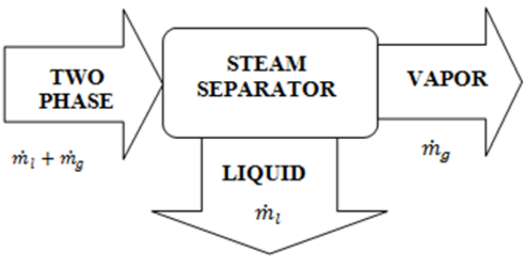

FIGURE 12: Mass conservation for a steam separator

The mass flowrate of fluid coming from the separator and going to the turbine is given by:

$$\dot{m}_9 = x_8 \dot{m}_8 \tag{3}$$

$$\dot{m}_9 = \dot{m}_{11} \tag{4}$$

Then, the mass flowrate of the separated water from the separator to the re-injection well may be written as:

$$\dot{m}_{10} = (1 - x_8)\dot{m}_8 \tag{5}$$

3.3 Demister process

The demister protects the turbine from moisture droplets in the steam from the separator. The liquid entrained in the steam can cause scaling and/or erosion in several components. The vapour that exits the separator contains very small moisture droplets. Due to condensation and transport time, droplet sizes increase. The demister eliminates and removes all the remaining condensed water drops in the steam and any solid dust that could travel together with the steam. The mass flow rate of the fluid (at point 13) going to the turbine is given by

$$\dot{m}_{13} = \dot{m}_{11} - \dot{m}_{14} \tag{6}$$

3.4 Turbine expansion process

The main component of a geothermal power plant is the turbine. The saturated steam coming from the separator enters from the demister. The difference in pressure between the entrance and the exit of the turbine makes it possible to extract mechanical energy from the steam flow. The mechanical energy is then partially transformed into electric energy by a generator coupled with the turbine. The capacity of the turbine is a fundamental factor in the design of a geothermal power plant. In an ideal turbine, the process is considered isentropic (the entropy is constant). The isentropic turbine efficiency is defined as:

$$\eta_t = \frac{h_{13} - h_{15}}{h_{13} - h_{15s}} \tag{7}$$

The efficiency of the turbine is assumed in this case to be 85%. The mechanical turbine power is defined as:

$$\dot{W} = \dot{m}_{13}(h_{13} - h_{15}) \tag{8}$$

The generator efficiency is assumed to be 75%. The electrical power will be equal to the mechanical turbine power times the generator efficiency:

$$\dot{W}_t = \eta_g \dot{W} \tag{9}$$

3.5 Condenser

The function of the condenser is to condense the exhaust steam flowing from the turbine. Generally, there are two ways to perform condensation. The first is direct-contact (to mix the cooling water and the steam) and the other is to cool the steam without mixing. In a water cooled condenser, the cooling water passes through the heat exchanger (Figure 13) and removes heat from the steam. An energy balance for the heat exchanger gives:

$$\dot{m}_{15}(h_{15} - h_{18}) = \dot{m}_{17}(h_{16} - h_{17}) \tag{10}$$

3.6 Vacuum pump

The particularity of geothermal steam compared with that from conventional thermal power plants is the presence of non-condensable gases (NCGs), sometimes in large amounts. This leads to problems in the condenser since the steam is condensed to water and pumped out as a liquid, but the gases stay in a gaseous form. The NCGs cause power plant inefficiencies that result in an increase in the condenser pressure. It is important to remove the non-condensable gases that otherwise accumulate in the system. A vacuum pump is used to evacuate NCGs from the condenser. The power of the vacuum pump is calculated by the following equation (Cengel and Boles, 2006):

$$P_{Vpump} = \left[\frac{\gamma}{\gamma - 1}\right] \frac{\dot{m}_g R_u T_{cond}}{\eta_{Vpump} M_{gas}} \left[\left(\frac{P_{atm}}{P_{cond}}^{\left(1-\frac{1}{\gamma}\right)}\right) - 1\right] \tag{11}$$

where P_{Vpump} = The power of the pump (kW);
γ = $C_{p,gas}/C_{v,gas}$;
$\dot{m}_g$ = The mass flowrate of the gas (kg/s);
R_u = 8.314 kJ/(kmol K), the universal gas constant;
T_{cond} = The temperature of the condensable in (K);
η_{Vpump} = The efficiency of the pump;
M_{gas} = The molar mass of the gas; and
P_{atm} *and* P_{cond} = The atmospheric and condenser pressures in bar_a, respectively.

3.7 Cooling tower process

Power plants invariably discharge considerable energy to their surroundings by heat transfer. The large quantities of waste heat that are generated are often discarded into nearby lakes or rivers. This can involve excessive heating and may disrupt life-forms. There are several methods available to deal with this, most notably cooling towers which provide an alternative in locations where sufficient

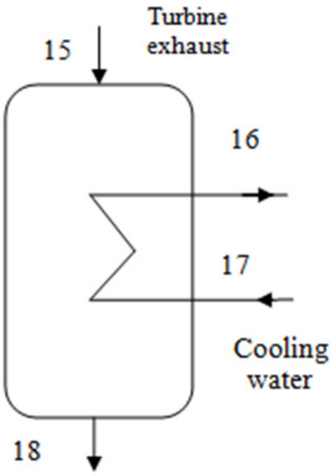

FIGURE 13: Condenser with heat exchange

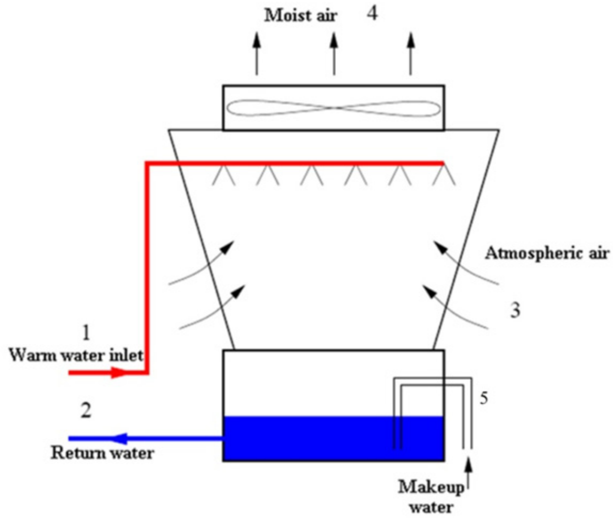

FIGURE 14: Mechanical induced draft wet cooling tower (modified from Pálsson, 2010)

cooling water cannot be obtained from natural sources. Cooling towers can operate by natural or forced convection. Also they may be counter-flow, cross-flow, or a combination of these.

We consider here a mechanical induced draft wet cooling tower, where air is forced in counter-flow configurations against flowing water (Figure 14). The warm water to be cooled enters at 1 and is sprayed from the top of the tower. The falling water usually passes through a series of baffles intended to keep it broken up into fine drops to promote evaporation. Atmospheric air is drawn in at 3 by the fan and flows upward, counter to the direction of the falling water droplets. As the two streams interact, a small fraction of the water stream evaporates into the moist air, which exists at 4 with a greater humidity ratio than the incoming moist air at 3.

Since some of the incoming water is evaporated into the moist air stream, an equivalent amount of water is added at 5 so that the return mass flow rate of the cool water equals the mass flow rate of the warm water entering at 1. This water, in addition to compensating for evaporation and drift, keeps the concentration of salts and other impurities down.

The cooled water is collected at the bottom of the tower and pumped back to the condenser to absorb additional waste heat. Make-up water must be added to the cycle to replace the water lost to evaporation and air draft. To minimise the water carried away by the air, drift eliminators are installed in the wet cooling tower above the spray section. The air circulation in the cooling tower is provided by fans; therefore, it is classified as a forced-draft cooling tower (Cengel and Boles, 2006).

For operation at steady state, mass balances for dry air and water and an energy balance on the overall cooling tower provide information about cooling tower performance (Moran and Shapiro, 2009).

Relative humidity is denoted as:

$$\Phi = \frac{P_v}{P_s} \tag{12}$$

where P_v = Partial pressure of water vapour in the air; and
P_s = Partial pressure of water vapour that would saturate the air at its temperature.

The humidity ratio is defined as:

$$\omega = \frac{M_v \Phi P_s}{M_a (P - \Phi P_s)} \tag{13}$$

where M_a and M_v are the molar masses of the dry air and the water.

The ratio of the molecular weight of water to that of dry air is approximately 0.622, leading to the revision of Equation 13 to the following form:

$$\omega = 0.622 \frac{P_v}{(P - P_v)} \tag{14}$$

The required mass flow rate can be found from mass and energy rate balances. Mass balances for the dry air and water individually reduce at steady state to:

$$\dot{m}_{a3} = \dot{m}_{a4} \text{ (Dry air)}$$

$$\dot{m}_1 + \dot{m}_5 + \dot{m}_{v3} = \dot{m}_2 + \dot{m}_{v4} \text{ (Water)}$$

where indices refer to number labels in Figure 12.

The common mass flow rate of the dry air is denoted as $\dot{m}_a$. Since $\dot{m}_1 = \dot{m}_2$, the second of these equations becomes:

$$\dot{m}_5 = \dot{m}_{v4} + \dot{m}_{v3}$$

With $\dot{m}_{v3} = \omega_3 \dot{m}_a$ and $\dot{m}_{v4} = \omega_4 \dot{m}_a$

$$\dot{m}_5 = \dot{m}_a (\omega_4 - \omega_3)$$

Accordingly, the two required mass flow rates, $\dot{m}_a$ and $\dot{m}_5$, are related by this equation. Another equation relating to the flow rates is provided by the energy rate balance.

$$\dot{m}_1 h_{w1} + \dot{m}_5 h_{w5} + \dot{m}_a h_{a3} + \dot{m}_{v3} h_{V3} = \dot{m}_2 h_{w2} + \dot{m}_a h_{a4} + \dot{m}_{v4} h_{v4}$$

Introducing $\dot{m}_1 = \dot{m}_2$, $\dot{m}_5 = \dot{m}_a(\omega_4 - \omega_3)$, $\dot{m}_{v3} = \omega_3 \dot{m}_a$ and $\dot{m}_{v4} = \omega_4 \dot{m}_a$, and solving leads to

$$\dot{m}_a = \frac{\dot{m}_1 (h_{w1} - h_{w2})}{h_{a4} - h_{a3} + \omega_4 h_{v4} - \omega_3 h_{v4} - (\omega_4 - \omega_3) h_{w5}} \tag{15}$$

3.8 Power of motor fan in cooling tower

To calculate the power of the fan P_{fan} (W) at the cooling tower, the equations are:

$$P_{fan} = \frac{\dot{v}_{air} \Delta P}{\eta_{fan} . 1000} \tag{16}$$

$$\dot{v}_{air} = \frac{\dot{m}_{air}}{\rho_{air,out}} \tag{17}$$

$$P_{motor,fan} = \frac{P_{fan}}{\eta_{motor,fan}} \tag{18}$$

where ΔP = The pressure drop (Pa);
$\dot{v}_{air}$ = The volume flowrate of air (m^3/s);
$\dot{m}_{air}$ = The mass flow of the air (kg/s);
$\rho_{air,out}$ = The density of the air out of the cooling tower in (kg/m^3);
η_{fan} = The efficiency of the fan; and
$\eta_{motor,fan}$ = The efficiency of the motor of the fan.

3.9 Power of pump

The following equations are used to calculate the power of the pump P_{pump} (W):

$$P_{pump} = \frac{\dot{v}_{water}\Delta P}{\eta_{pump}} \tag{19}$$

$$\dot{v}_{water} = \frac{\dot{m}_{water}}{\rho_{water}} \tag{20}$$

$$P_{motor,pump} = \frac{P_{pump}}{\eta_{motor,pump}} \tag{21}$$

where ΔP = The pressure drop (Pa);
$\dot{v}_{water}$ = The volume flowrate of water (m^3/s);
$\dot{m}_{water}$ = The mass flow of the water (kg/s);
ρ_{water} = The density of water (kg/m^3);
η_{pump} = The efficiency of the pump; and
$\eta_{motor,pump}$ = The efficiency of the motor of the pump.

3.10 Output of the power plant

The output of the power plant is found by the following equations (see Figure 8 for reference):

$$W_{water,pump} = W_{motor,pump1} + W_{motor,pump2} + W_{motor,pump3} \tag{22}$$

$$Auxiliary\ power = W_{motor,Vpump} + W_{water,pump} + W_{motor,fan} \tag{23}$$

$$W_{net\ output} = W_{turbine} - (Auxiliary\ power) \tag{24}$$

4. CALCULATIONS AND DISCUSSION OF RESULTS

4.1 The specific case of Djibouti

Cooling constraints for the Asal site:
Temperature minimum: 16°C
Temperature maximum: 48°C
Relative humidity yearly range: 40-90%
Average temperature during cold season: 26°C
Average temperature during hot season: 33°C
Red Sea water temperature range 22-34°C

Determining the temperature of the cooling fluid (T_cw_1):
In Djibouti, the highest ambient temperature throughout the year reaches 48°C with an average relative air humidity of 65%. The wet bulb temperature calculated from the psychometric chart is 41°C. Because of a limited source of cooling water, a wet cooling tower was chosen. With a wet cooling tower, the "cold water" temperature approaches the "wet bulb" temperature. Realistically the best approach temperature (hot day) is about 3°C above the wet bulb temperature (Páll Valdimarsson, pers. comm.). Therefore, in this calculation a "cold water" temperature of 44°C was used.

Limitations of the condenser pressure:
The circulating water inlet temperature should be sufficiently lower than the steam saturation temperature to result in a reasonable value of TTD. It is usually recommended that ΔT_i should be between 11 and 17°C and that TTD should not be less than 2.8°C (El-Wakil, 1984). By using the possible cooling water input (T_cw_1) from the wet cooling tower at 44°C and assuming a minimum approach in the condenser (ΔT_i) by 12°C (Figure 15), the temperature of the condensate T_cw_2=T_cw_1+ ΔT_i = 56°C. The condenser pressure is, then, the saturated pressure at this temperature plus the pinch temperature 5°C. Based on these criteria and environmental conditions, the condenser pressure is 0.2 bars.

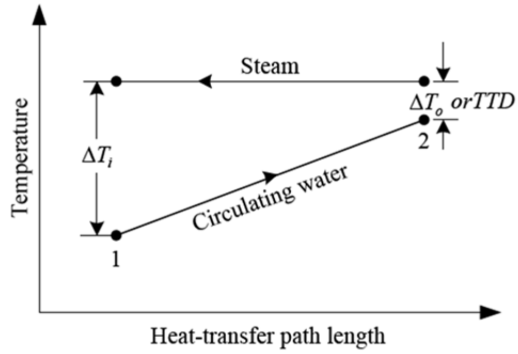

FIGURE 15: Condenser temperature distribution

4.2 Optimum separator pressure

The optimum separator pressure is defined as the pressure at which the power plant's output is maximised. To find the optimum pressure of the separator, the wet-bulb temperature is kept constant and the power plant output is calculated for different separator pressures. The separator pressures were varied between 4 and 17.7 bars for different wet-bulb temperatures of the surroundings.

The results of the calculations with the plant output power versus the separator pressures for different wet-bulb temperature are shown in Figure 16. The uppermost curve gives the highest power output. It is the curve calculated by a condenser pressure of 0.06 bars or by a wet-bulb temperature of 16°C. The highest power output in this curve is 54,583 kWe, given by a separator pressure of 9 bars. The 9 bars separator pressure is then calculated to be the optimum separator pressure, giving the maximum output power. However, it cannot be used in the case of the Asal geothermal power plant because of the problem of deposition explained above (see sections 2.4.1 and 2.4.2). In this case, the separator pressure selected is 17.7 bars. With this pressure, the scaling was minimised and there was no decrease in the flowrate in a three month test period (Figure 8). The power output (51,643 kWe) generated with 17.7 bars is lower than that calculated with 9 bars in the same condition. The calculations for turbine power, output power and auxiliary power (kWe) for different condenser pressures at the 17.7 bars separator pressure are summarised in Table 5.

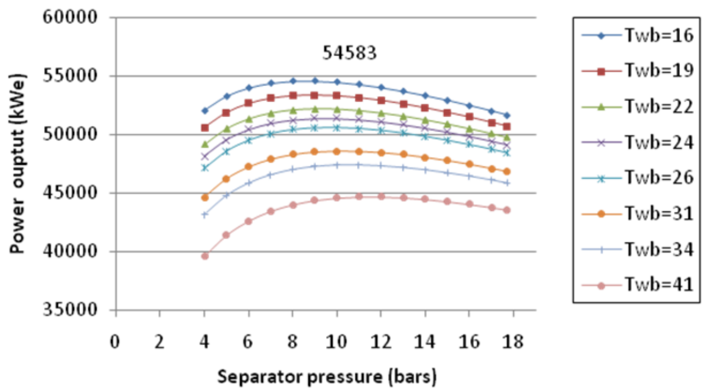

FIGURE 16: Separator pressure vs. power output

The condenser pressure has an interrelationship with the wet-bulb temperature (Table 5). According to Table 5, the turbine and output powers decrease as the wet-bulb temperature increases. But the gap between the turbine power and the output power decreases when the pressure of the condenser decreases due to lower auxiliary power needs, as seen in Figure 16 and Table 5.

TABLE 5: Turbine, output and auxiliary powers for 17.7 bars separator pressure

Wet-bulb temperature (°C)	Condenser pressure	Turbine power	Output power	Auxiliary power
16	0.06	55,603	51,643	3,959
19	0.07	54,430	50,694	3,736
22	0.08	53,277	49,747	3,529
24	0.09	52,505	49,104	3,401
26	0.10	51,736	48,457	3,279
34	0.15	48,697	45,843	2,855
41	0.21	46,083	43,532	2,551

After deducting 0.01 bars from the separator pressure due to lost pressure in the demister, the optimum inlet pressure of the turbine is obtained. Hence, the optimum inlet pressure of the turbine is 17.69 bars.

4.3 Wet-bulb temperature

The wet-bulb temperature was varied between 16 and 42°C with the separator pressure kept constant at 17.7 bars. The output power increased when the wet-bulb temperature decreased (Figure 17). In Equation 24, the power is a function of the auxiliary power and the auxiliary power is a function of the fan power, vacuum pump and water pump. The fan power and the vacuum pump power decrease when the wet-bulb temperature increases.

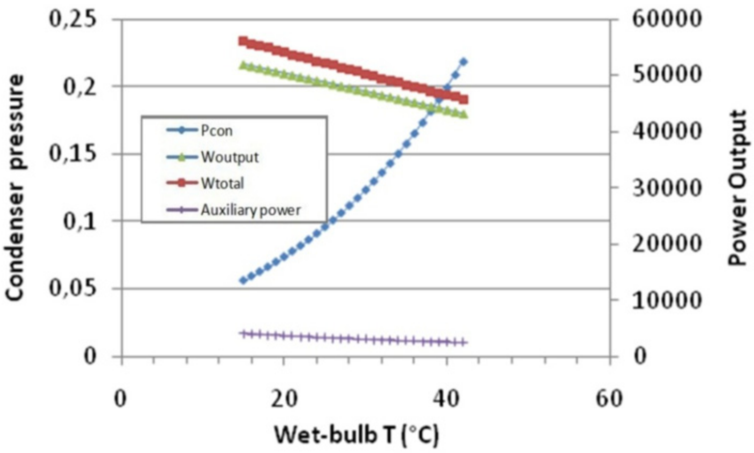

FIGURE 17: Wet-bulb temperature vs. power output (kW) and condenser pressure (bar)

4.4 Optimum condenser pressure

The optimum pressure of the condenser is the pressure in the condenser at which the output from the power plant is maximised. The output from the power plant is calculated for different pressures in the condenser while the pressure in the steam separator is kept constant. The results of these calculations are shown in Figure 18, where the output of the plant is plotted vs. pressure in the condenser for

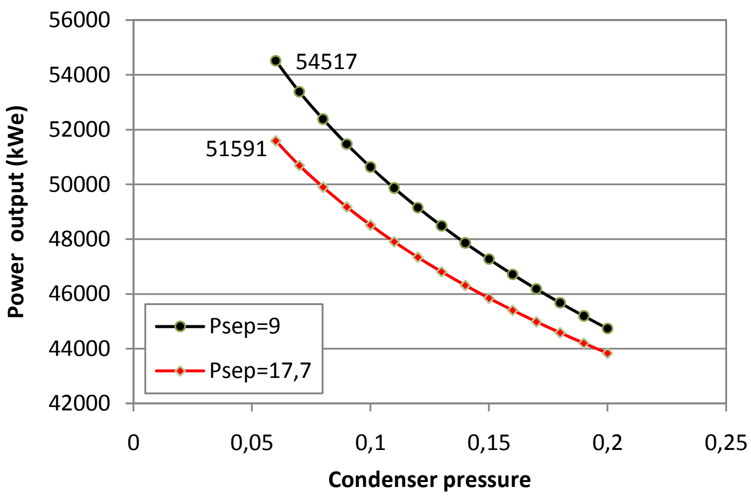

FIGURE 18: Condenser pressure (bar) vs. power output

different pressures in the separator. The results show that the optimum pressure in the condenser is 0.06 bars, and the highest output of the power plant is 54.517 kWe when the pressure in the separator is 9 bars. But for the curve of 17.7 bars separator pressure, the optimum condenser pressure is also 0.06 bars. This condenser pressure can only by obtained when the wet-bulb temperature of the power plant's surroundings is at its minimum of 16°C. As the wet-bulb temperature increases, so does the pressure in the condenser.

4.5 Comparison of cooling water supply systems

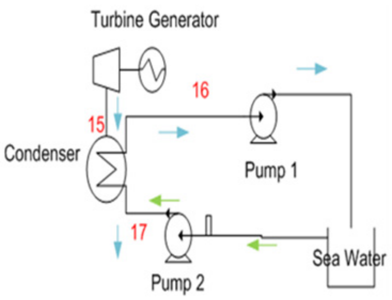

FIGURE 19: Part of the schematic of the power plant

Here, the system was calculated without a cooling tower (Figure 19). The hot water from the condenser through the heat exchanger is rejected directly into the Red Sea. Using a variable Red Sea temperature of 22-34°C and a constant separator pressure of 17.7 bars, the pressure in the condenser is calculated (Table 6), as is the output power from the plant (Table 7 and Figure 20). The output power with the cooling tower is bigger than that calculated without a cooling tower. When the Red Sea temperature increases, the gap between the two curves becomes larger. This difference lies in the auxiliary power; the turbine power in the two cases is the same.

TABLE 6: Correlation between pressure in condenser, Red Sea temperature and wet-bulb temperature

Pressure condenser (Bars)	**Red Sea temperature (°C)**	**Wet-bulb temperature (°C)**
0.06997	22	19
0.07381	23	20
0.07784	24	20.97
0.08205	25	21.97
0.08646	26	22.97
0.09108	27	23.97
0.0959	28	24.97
0.1009	29	25.97
0.1062	30	26.97
0.1117	31	27.97
0.1174	32	28.96
0.1234	33	29.97
0.1297	34	30.97

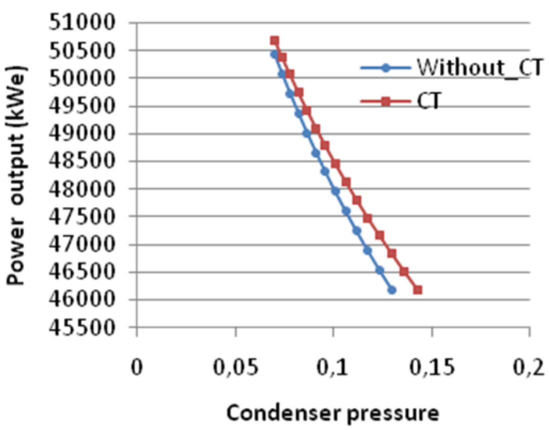

FIGURE 20: Comparison of the output power with cooling tower and without it

The cooling tower adds to the cost during installation but is ultimately more profitable over time and also more respectful of the environment.

TABLE 7: Comparison between output power with and without cooling tower

Without cooling tower			With cooling tower			
Wauxiliary	**Wturbine**	**Woutput**	**Wauxiliary**	**Wturbine**	**Woutput**	**Pressure condenser**
3,994	54,430	50,436	3,736	54,430	50,694	0.06997
3,962	54,041	50,079	3,665	54,042	50,376	0.07381
3,931	53,664	49,732	3,597	53,664	50,067	0.07784
3,901	53,277	49,376	3,530	53,277	49,747	0.08205
3,871	52,890	49,019	3,465	52,890	49,425	0.08646
3,842	52,505	48,663	3,402	52,504	49,103	0.09108
3,813	52,120	48,307	3,340	52,120	48,780	0.0959
3,784	51,736	47,952	3,280	51,739	48,459	0.1009
3,756	51,353	47,597	3,222	51,354	48,132	0.1062
3,728	50,971	47,243	3,165	50,972	47,807	0.1117
3,701	50,590	46,889	3,110	50,593	47,483	0.1174
3,674	50,210	46,536	3,056	50,213	47,156	0.1234
3,648	49,831	46,183	3,004	49,831	46,827	0.1297

5. CONCLUSIONS

The work presented in this report contributes to the modelling of a geothermal power plant and facilitates seeing the effects of the outside temperature (wet-bulb temperature) on the system and its subsequent reactions. When the wet-bulb temperature increases, the condenser pressure increases also. The increase of the pressure in the condenser involves the reduction of the net power output. The net output power decreases linearly with wet-bulb temperature increase. Based upon the thermodynamic analysis of the power plant design, calculations and recommendations, a maximum power output of the plant is achieved by operating the condenser at 0.06 bars, given a separator pressure at 17.7 bars. At this design pressure, the turbine power would attain 55.6 MW and a power output of 51.6 MW. The auxiliary power for pumping, cooling tower fan and other equipment is 4 MW. The analysis of the comparison and the observation of the two cooling water supply systems conclude that a cooling tower adds to the cost of installation but is ultimately more profitable in the long term and is also more respectful to the environment than direct use of sea water. It is advised to enhance this survey with additional data (such as well productivity curves and elevation) in order to achieve a more realistic model.

ACKNOWLEDGEMENTS

I wish to express my sincere gratitude to the United Nations University – Geothermal Training Programme (UNU-GTP) and the Ministry of Energy and Natural Resources for giving me the opportunity to participate in the 32nd session of the UNU-GTP. My gratitude goes to Dr. Ingvar B. Fridleifsson, the Director of UNU-GTP, Mr. Lúdvík S. Georgsson, the Deputy Director of UNU-GTP, and Mr. Ingimar G. Haraldsson, Mr. Markús A.G. Wilde, Ms. Thórhildur Ísberg, and Mrs. Dorthe H. Holm of UNU-GTP, for their guidance, assistance and care throughout the course. My special thanks go to my supervisor, Dr. Gudrún Saevarsdottir, assistant professor of Reykjavik University, and Ms. Marta R. Karlsdóttir MSc, lecturer at the University of Iceland, for their dedicated support and guidance during project preparation, research and writing, which made it possible for me to complete this report. To all UNU Fellows, I am grateful for your company, support and the sharing we had during the six months of training. Last but not least, I am grateful to my family, for their endurance, emotional support, prayers, and encouragement throughout the course and my stay in Iceland.

NOMENCLATURE

A	= Area (m^2);
H	= Enthalpy fluid (kJ/kg);
T	= Temperature (⁀C);
A1	= Well Asal 1;
A3	= Well Asal 3;
A4	= Well Asal 4;
A5	= Well Asal 5;
A6	= Well Asal 6;
NCG	= Non-condensable gas; and
CT	= Cooling tower.

REFERENCES

Aquater, 1989: *Djibouti geothermal exploration project Republic of Djibouti, final report*. Aquater, report, 159 pp.

Ármannsson, H., and Hardardóttir, V., 2010: Geochemical patterns of scale deposition in saline high temperature geothermal systems. In: Birkle, P., and Torres-Aivarado, I.S. (eds.), *Water-Rock Interaction 14,* CRS Press, 133-136.

Árnason, K., Björnsson, G., Flóvenz, Ó.G., and Haraldsson, E.H., 1988: *Geothermal resistivity survey in the Asal Rift in Djibouti.* Orkustofnun, report OS-88301/JHD-05 prepared for UND-OPS and ISERT, vol. I, 48 pp.

Bandoro, R.S., 2006: Thermodynamic analysis of preliminary design of power plant unit I Patuha, West Java, Indonesia. Report 7 in: *Geothermal Training in Iceland 2006*. UNU-GTP, Iceland, 83-119.

Cengel, Y.A., and Boles, M.A., 2006: *Thermodynamics: an engineering approach* (5^{th} edition). McGraw-Hill, Inc, New York, 645 pp.

El-Wakil, M.M., 1984: *Powerplant technology.* McGraw-Hill, Inc, USA, 859 pp.

Elmi H., D., 2005: Analysis of geothermal well test data from the Asal rift area, Republic of Djibouti. Report 6 in: *Geothermal Training in Iceland 2005*. UNU-GTP, Iceland, 39-59.

Elmi, H.D., and Axelsson, G., 2010: Geothermal resources in the Asal region, republic of Djibouti: an update with emphasis on reservoir engineering studies. *Geothermics, 39-3*, 220-227.

Jalludin, M., 2009: State of knowledge of the geothermal province of the Republic of Djibouti*. Paper presented at Short Course IV on Exploration for Geothermal Resources organized by UNU-GTP, KenGen and GDC, Lake Naivasha, Kenya,* 14 pp.

Moran, M.J., and Shapiro, H.N., 2009: *Fundamentals of engineering thermodynamics* (6^{th} edition). John Wiley & Son, Inc., NY, 694 pp.

Pálsson, H., 2010: *Utilisation of geothermal energy for power production*. UNUGTP, Iceland, unpublished lecture notes.

Virkir-Orkint, 1990: *Djibouti. Geothermal scaling and corrosion study.* Virkir-Orkint, Reykjavík, report, 109 pp.

APPENDIX I: Models, equations and calculations: Asal geothermal power plant (EES-program)

1. Comparison of two models of the power plant

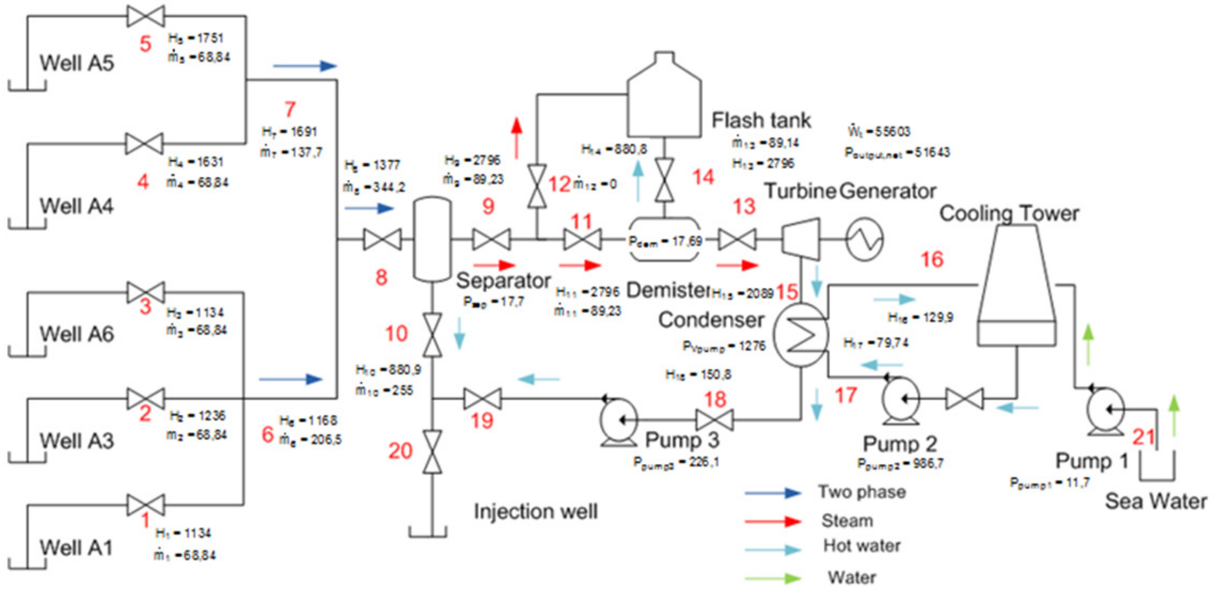

FIGURE 1: Schematic of the power plant with cooling tower

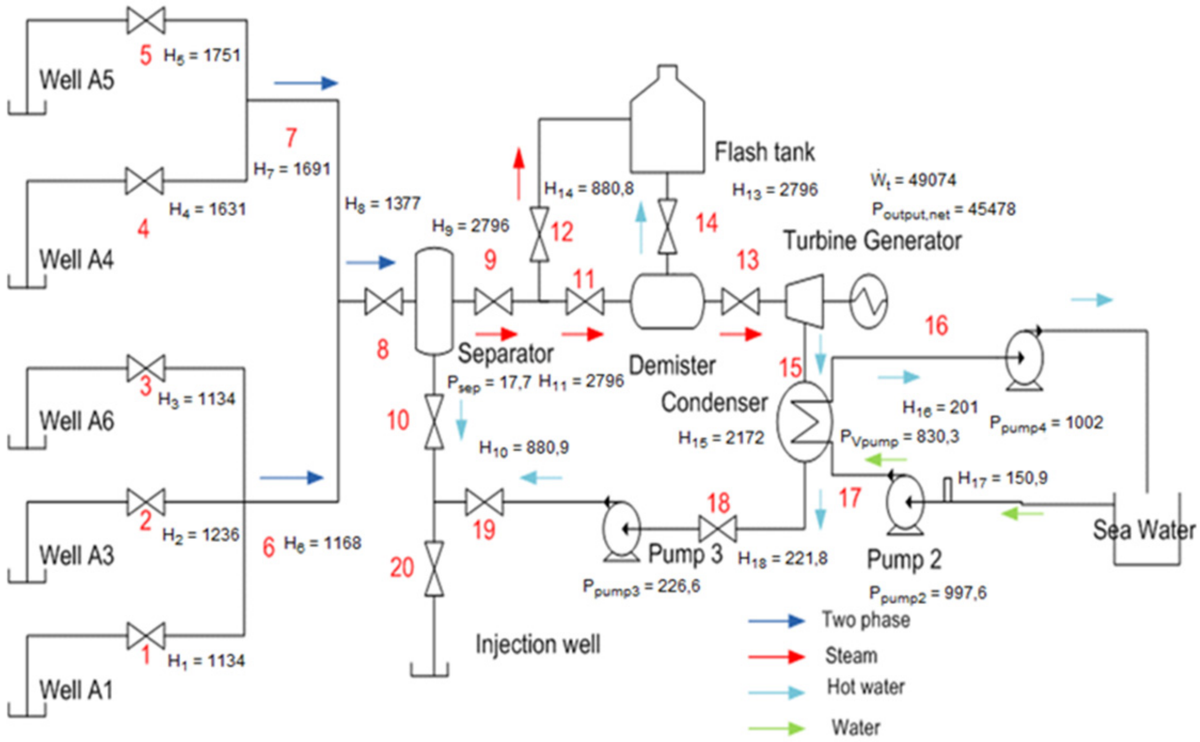

FIGURE 2: Schematic of the power plant without cooling tower

2. Equations of the model

```
{Production Wells conditions}

WHP[1]=17,7
WHP[2]=WHP[1] "17,7"
WHP[3]=WHP[1] "17,7"
WHP[4]=WHP[1] "17,7"
WHP[5]=WHP[1] "17,7"

m_dot[1]=((-3,6279*(WHP[1])^2)+(89,234*WHP[1])-195,03)*(1000/3600)
m_dot[2]=((-3,6279*(WHP[2])^2)+(89,234*WHP[2])-195,03)*(1000/3600)
m_dot[3]=((-3,6279*(WHP[3])^2)+(89,234*WHP[3])-195,03)*(1000/3600)
m_dot[4]=((-3,6279*(WHP[4])^2)+(89,234*WHP[4])-195,03)*(1000/3600)
m_dot[5]=((-3,6279*(WHP[5])^2)+(89,234*WHP[5])-195,03)*(1000/3600)

T[1]=260
T[2]=280
T[3]=260
T[4]=345
T[5]=359

H[1]=Enthalpy(Water;x=0;T=T[1])
H[2]=Enthalpy(Water;x=0;T=T[2])
H[3]=Enthalpy(Water;x=0;T=T[3])
H[4]=Enthalpy(Water;x=0;T=T[4])
H[5]=Enthalpy(Water;x=0;T=T[5])

{Separator Inlet}

m_dot[7]=m_dot[4]+m_dot[5]
m_dot[6]=m_dot[1]+m_dot[2]+m_dot[3]
H[6]=(H[1]*m_dot[1]+H[2]*m_dot[2]+H[3]*m_dot[3])/(m_dot[1]+m_dot[2]+m_dot[3])
H[7]=(H[4]*m_dot[4]+H[5]*m_dot[5])/(m_dot[4]+m_dot[5])
m_dot[8]=m_dot[6]+m_dot[7]
H[8]=(H[6]*m_dot[6]+H[7]*m_dot[7])/(m_dot[6]+m_dot[7])

{Separator outlet}

P_sep=17,7  "WHP[1]*(0,9)"
P[9]=P_sep
H[9]=Enthalpy(Water;x=1;P=P[9])
P[10]=P[9]
H[10]=Enthalpy(Water;x=0;P=P[10])
x_8=(H[8]-H[10])/(H[9]-H[10])
m_dot[10]=(1-x_8)*m_dot[8]
m_dot[9]=x_8*m_dot[8]

{Demister}

m_dot[12]=0
m_dot[11]=m_dot[9]-m_dot[12]
H[11]=H[9]
delta_p11=0,01                                        "Drop pressure at point 11"
```

```
P_dem=P_sep-delta_p11
P[13]=P_dem
P[14]=P_dem
H[13]=Enthalpy(Water;x=1;P=P[13])
H[14]=Enthalpy(Water;x=0;P=P[14])
x_11=(H[11]-H[14])/(H[13]-H[14])
m_dot[14]=0,001*m_dot[11]
m_dot[13]=m_dot[11]-m_dot[14]

{Turbine and condenser}

P_con=P_sat(Water;T=T_con)
P[15]=P_con
s_15_s=Entropy(Water;P=P_dem;x=1)
H_15_s=Enthalpy(Water;S=s_15_s;P=P[15])
eta_t=0,85                                   "Turbine efficiency"
eta_t=(H[13]-H[15])/(H[13]-H_15_s)
W_dot=m_dot[13]*(H[13]-H[15])              "Mechanical Turbine power"
eta_total=0.75                                "Generator efficiency"
W_dot_t=(eta_total/eta_t)*W_dot            "Turbine-Generator  power net"

P[18]=P_con
H[18]=Enthalpy(Water;x=0;P=P[18])
T[18]=Temperature(Water;P=P[18];x=0)
m_dot[15]=m_dot[13]
m_dot[18]=m_dot[13]

{Gas compressor}

NCG=0,025
M_v=MolarMass(Steam_IAPWS)
M_a=MolarMass(CO2)
m_dot_a=NCG*m_dot[13]
T_s=T[18]-2
P_s=P_sat(Steam_IAPWS;T=T_s)
m_dot_v=(M_v*P_s)*m_dot_a/(M_a*(P_con-P_s))

c_p_a=SpecHeat(CO2;T=T_s)
c_p_v=SpecHeat(Steam_IAPWS;T=T_s;x=1)
c_p=c_p_a+((c_p_v-c_p_a)*((P_s*M_v)/(P_con*(M_a+M_v))))
R_a=isIdealGas(CO2)
R_v=isIdealGas(Steam_IAPWS)
R=R_a+((R_v-R_a)*((P_s*M_v)/(P_con*(M_a+M_v))))
delta_h=c_p*T_s*((p_atm/P_con)^(R/c_p)-1)
eta_comp=0,85
W_c=(m_dot_a+m_dot_v)*delta_h/eta_comp

{Vacum pump}

m_dot_g=(NCG)*m_dot[13]
R_u=8,314
```

```
eta_V_pump=0,4
M_gas=MolarMass(CO2)
p_atm=1
C_p_gas=CP(CO2;T=T_con)
C_v_gas=CV(CO2;T=T_con)
gamma=C_p_gas/C_v_gas
P_Vpump=(gamma/(gammA1))*((m_dot_g*R_u*(T_con+273,1))/
(eta_V_pump*M_gas))*(((p_atm/P_con)^((gammA1)/gamma))-1)
eta_motor_Vpump=0,85
P_motor_Vpump=P_Vpump/eta_motor_Vpump

{Cooling tower}
.
.
.
.
.

"Results"

P_water_pump=P_motor_pump3+P_motor_pump2+P_motor_pump1

Auxiliary_power=P_motor_Vpump+P_water_pump+P_motor_fan
P_output_net=W_dot_t-(P_motor_Vpump+P_water_pump+P_motor_fan)
```